

45 Km horizontal path optical link demonstrations

Abhijit Biswas, Malcolm W. Wright, Babak Sani, Norman A. Page

*Optical Communications Group
Jet Propulsion Laboratory, California Institute of Technology,
4800 Oak Grove Drive, Pasadena, CA 91109-8099*

ABSTRACT

Observations made during a mountain-top-to-mountain-top horizontal optical link demonstration are described. The optical link spans a range of 45 Km at an average altitude of 2 Km above sea level. A multi-beam beacon comprised of eight laser beams emerging from multi-mode fiber coupled lasers (780 nm) are launched through a 0.6 m diameter telescope located at the JPL Table Mountain Facility (TMF) in Wrightwood, California. The multi-beam beacon is received at Strawberry Peak located in the San Bernadino Mountains of California. The NASA, JPL developed optical communications demonstrator (OCD) receives the beacon, senses the atmosphere induced motion and using an upgraded fine steering loop compensates the re-transmission of a communications laser beam (852 nm, 400 Mbps) to TMF. The eight-beam beacon allowed a four reduction in normalized irradiance or scintillation index. This in turn was sufficient to eliminate beacon fades sensed by the OCD and allowed the fine steering loop performance evaluation. The uncompensated tracking error was determined to be 2.2 – 3 μ rad compared to a model prediction of 3.4 μ rad. The paper also discusses various auxiliary observations made during the campaign.

1. INTRODUCTION

Free-space optical communications technology is being developed at JPL in order to service to an expanding set of future NASA missions. Higher data rates with lower mass and power requirement are the key sought after improvements driving the technology development. Furthermore, the potential for significant bandwidth expansion in an unregulated portion of the electromagnetic spectrum is an added benefit. As a part of the early end-to-end systems level evaluation of free-space optical communications technology, ground-to-ground horizontal path optical link demonstrations were initiated in 1998.^{1,2} This report presents results of a follow-on ground-ground demonstration conducted during the summer of 2000.

As before the link was established between Strawberry Peak (SP), Lake Arrowhead, California and the NASA, JPL, Table Mountain Facility (TMF) in Wrightwood, California. The optical communications demonstrator^{3,4} (OCD), a NASA, JPL patented laboratory prototype terminal was located at SP, while a 0.6 m telescope at TMF served as the ground station. The main objectives of the demonstration were: (i) characterization of a multi-beam beacon comprised of 8 mutually incoherent laser beams and (ii) evaluation of an upgraded fine steering loop implemented in OCD. Additionally, a re-assessment of link uncertainties and end-to-end link performance evaluation was also carried out.

Compared to horizontal path links exceeding 10Km range, space-to-ground links for satellite laser communications, involve beam propagation through lower air mass. Consequently, the impact of atmospheric turbulence effects is less severe than that encountered on horizontal links. On the other hand, space-to ground links usually involve dynamic tracking and pointing strategies in order to maintain line-of-sight and compensate for space platform vibrations and jitter. Ground to geo-stationary (GEO) orbiting spacecraft is an exception where the line-of-sight is also essentially static. The transmitting aperture also being "immersed" in the atmosphere for horizontal links gives rise to another noteworthy difference. A serious consequence of this is beam wander of the laser beam exiting the transmitter and focal spot distortions of the beacon received by the transmitter. These differences complicate a direct comparison between horizontal and space-to-ground links. Notwithstanding these important differences, we believe that horizontal link demonstrations do provide a cost-effective early systems evaluation and operational experience.

The operational details along with a description of the setups used at either end of the link are briefly described in section 2. Results, including comparisons with theoretical predictions, are described in section 3, followed by conclusions in section 4.

2. OPERATIONS AND SETUP

2.1 Operational Scenario

Figure 1 shows a sectional view of the intervening terrain along the 46-Km link. The optical path ~2 Km above sea level, provides relatively favorable atmospheric turbulence as evidenced by numerous measurements and models⁵. The optical link was initiated by broadcasting a multi-beam beacon from the 0.6-m aperture telescope at TMF to SP. The beacon was continuous wave (cw) with a 780 nm wavelength, while OCD retransmitted a communications signal at 852 nm. At SP, a sturdy tripod was used for mounting OCD. The upgraded OCD (section 2.3) control system was not equipped with coarse pointing capability, thus manual adjustment of the azimuth elevation mount was used to initially acquire the beacon following the procedure about to be described.

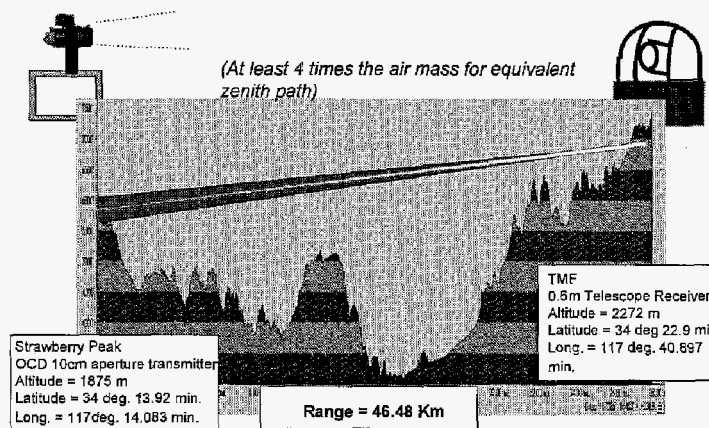


Figure 1 Showing a sectional view of the intervening terrain between Table Mountain Facility (TMF) and Strawberry Peak (SP).

Initial alignment relied upon knowledge of the 0.6-m TMF telescope settings required for locating SP. Under night-time conditions used during the demonstration, a co-bore-sighted spotting telescope (0.15 m aperture) allowed easy validation of the telescope pointing. Once the 0.6-m telescope was pointed to SP a multi-beam beacon (780 nm) comprised of 8 co-aligned beams (see 2.2 for details) was broadcast from TMF to SP.

Acquiring the beacon in OCD's relatively narrow ~1 mrad field-of-view (FOV) required careful manual adjustment. To ease this process the 852 nm communications laser beam transmitted by OCD was turned on and from TMF it was monitored through the intensified camera video monitor as OCD was manually adjusted to point toward TMF. Once this 852 nm laser spot was sensed at TMF, it was relatively easy to guide the manual adjustments of the OCD coarse azimuth and elevation mount in order to walk the beam in. Prior to excessive saturation of the intensified camera hand-off to power-meter sensor located at the Coudé focus of the 0.6-m telescope was possible. The power received at TMF was increased by further coarse adjustments of OCD at SP. Finally, the OCD fine steering mirrors were electronically stepped to maximize the power received at TMF. The latter automatically resulted in acquisition and centering of the beacon spot on OCD's tracking sensor.

Once aligned the beacon irradiance was adjusted to a reasonable level so that the OCD tracking sensor would not display fades or surges. Beacon spot sizes were recorded as was the acquired beacon intensity and centroid. OCD's fine tracking loop was initiated and both the beacon and transmit laser spot intensities and centroids were simultaneously recorded during tracking.

In addition to OCD, a pair of receiving 9-cm aperture Maksutov-Cassegrain spotting telescopes retrofitted with avalanche photodiodes (APD) in their focal plane, and mounted on separate tripods was used to receive the beacon. The alignment in this case was accomplished by first sending a helium neon (He:Ne) laser through the TMF telescope nominally co-aligned to the outgoing beacon. This eye-safe He:Ne laser aided the coarse alignment of the spotting telescopes followed by finer alignment to maximize the 780 nm signal sensed by the

APD detectors. The spotting scopes were used to record irradiance fluctuations of the beacon. This was performed by broadcasting different number of beams so that the multi-beam averaging could be evaluated.

All the laser beams transmitted through the atmosphere were at irradiance levels well below the maximum permissible exposure (MPE) levels at the exit apertures specified by the ANSI Z-36.1 eye-safety standards.

2.2 TMF Setup

A 0.6-m Richey-Chretien telescope at TMF was used for broadcasting the beacon (780 nm), as well as, receiving the communications signal (852 nm). The telescope Coudé configuration was used with a transmit-receive optical assembly located in the Coudé room.

Figure 2a shows a schematic representation of the multi-beam beacon laser assembly. The laser sources used were four thermoelectrically (TEC) cooled fiber-coupled laser diodes (62.5 μm core diameter, 0.25 NA) emitting approximately 25-mW each at 780 nm. The output of each laser was split using a 50/50 multi-mode fiber splitter and then collimated. The resulting eight collimated beams were co-aligned in a ring pattern using the prism assembly. The co-propagating beams were then steered through a lens assembly chosen to match the telescope optical train and deliver the required beam divergence. This resulted in all eight beams uniformly

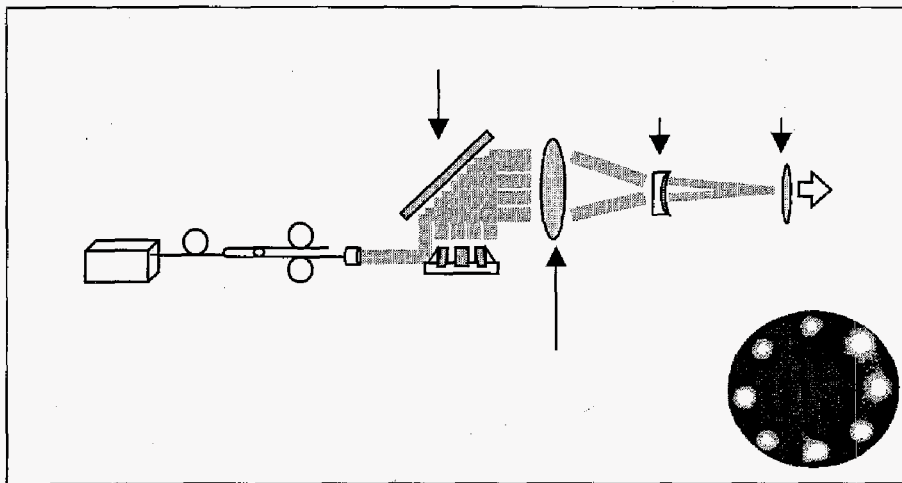


Figure 2 Block diagram of the multi-beam beacon assembly used to broadcast eight 780 nm laser beams to SP. Shown in the inset is a captured video image of the appearance of the beacon laser spots on the telescope dome inner wall.

diverging from the Coudé focus and incident in an annular pattern on the 0.6 m telescope primary mirror. A photograph of the 8-beam pattern projected on the telescope dome is shown in the inset of figure 2a. The lens assembly was designed to provide spots with a 100% energy diameter of 4.1-cm on the primary mirror corresponding to a nominal 120- μrad divergence per beam. The design was based on measured beam profiles emitted from the fiber core of the lasers. The actual beam profile emitted from the multi-mode fibers cannot be modeled exactly introducing variance in the beam divergences.

Figure 3a shows a schematic view of the overall transmit/receive optical train used in the TMF telescope Coudé room. The relative configuration of the beacon assembly is apparent. The transmit/receive optical paths are separated by a dichroic beam splitter. The received 852 nm signal is transmitted through the dichroic beam splitter and re-collimated. The collimated beam can be optionally split among three receiving channels by manipulating the flip mounted (curved arrow in Fig 3a) optical elements shown in figure 3a. The three receiving channels are for data, focal spot monitoring and pupil image of the telescope primary mirror. The data channel sensor is an APD with a 500 μm diameter active area, a bandwidth of 450-MHz and voltage conversion gain of 170 KV/W. The APD maximum noise equivalent power (NEP) is 0.6 nW (-61 dBm) at 450 MHz. The APD output is fed to a limiting amplifier requiring a minimum of 15-mV peak-to-peak signal. The limiting amplifier output is fed to a clock and data recovery circuit. Pupil images were acquired at video frame rates with varying exposure times (30, 20, 10, 5, 1 millisecond) using a CCD camera and frame-grabber. A second channel equipped with a CCD camera and frame grabber is used to record and monitor the focal spot size and its variations.

A power meter was used near the Coudé focus for measuring received power. Irradiance fluctuations were also measured at the same location using a photodiode (4 x 4 mm square), sampled at 1-5-KHz by a

digitizing oscilloscope. Finally, figure 3 also shows the He:Ne laser used for establishing the telescope bore-sight as well as transmitting to SP. Note that unlike the beacon the He:Ne beam is transmitted without any optical conditioning so that it exits the telescope with essentially the same divergence as the laser. This was approximately measured to be 800 μ rad. Other TMF setup details related to data acquisition are identical to descriptions provided in reference 1 and 2.

2.3 SP Setup

The SP setup has been previously described.^{1,2} An 852 nm optical-fiber-pigtailed diode capable of high speed (500 Mbps) on-off key modulation provides ~8 mW of average optical power to the OCD. Approximately 3-4 mW of optical power exits the telescope. The fine tracking control loop of OCD was upgraded. The upgrade consisted firstly, of replacing the General Scanning fine steering mirror (FSM) with one manufactured by Left Hand Design Corporation and secondly, of using upgraded software for the control loop.

Software for controlling the OCD's fine steering loop was upgraded and tested out using the Acquisition Tracking and Pointing (ATP) testbed at JPL. The upgrade features were the use of a new centroiding algorithm, and integration of the new fine steering mirror with properly designed filters. In addition, better real time diagnostics is supported. Thus for acquisition real time image and centroid data can be stored. During fine tracking real time beacon and transmit spot centroids can be stored for 5 seconds. The tracking sensor update frame rate used for fine tracking was 1 KHz.

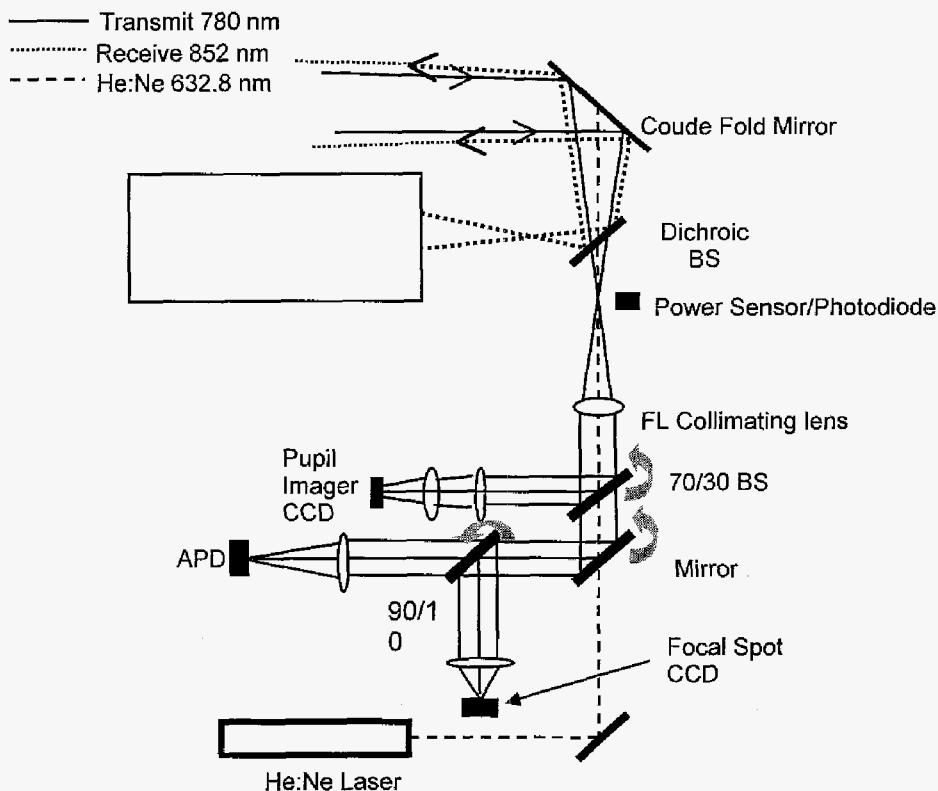


Figure 3 Overall Coudé room assembly used at TMF, the details of the receive train are shown the beacon (transmit) assembly was detailed in the previous figure

The auxiliary beacon monitoring spotting telescopes were retrofitted with avalanche photodiodes (APD's) to record the incoming beacon irradiance fluctuations. The 3mm diameter APD's were characterized in the laboratory and found to have a dynamic range 37-38 dB. They were also calibrated so that the measured signal could be converted into optical power.

3. RESULTS

3.1 Beacon Characterization

Beacon characterization consisted of validating: (i) the link budget (ii) the reduction in irradiance fluctuations (scintillation) due multiple beam averaging and (iii) the fade characteristics.

3.11 Beacon power received at SP

The largest source of uncertainty in predicting link budgets for a single beacon beam propagating from TMF to SP was the beam divergence (footprint at SP). The ill-defined beam profiles emerging from the multimode fibers contributed to this uncertainty. The TMF telescope was step scanned while recording power received by the spotting scopes at SP. The TMF telescope has an equatorial mount and therefore can be scanned only in hour angle (HA) and declination (DEC) in steps of $\sim 5 \mu\text{rad}$. Profiles for selected beams were measured on two different nights. The measured far field beacon profiles at SP were transformed from HA and DEC to azimuth and elevation angular widths at SP using standard co-ordinate transformation equations⁶. Table 1 summarizes the results

Table 1 A summary of the FWHM beam widths measured in HA and DEC and transformed to elevation and azimuth angular widths

Beam #1		Beam #5		Beam #3	
EI (μrad)	Az (μrad)	EI (μrad)	Az (μrad)	EI (μrad)	Az (μrad)
138	153	128	171	93	83

The beam footprints are elliptical with aspect ratios of 0.7 – 0.9. The full widths (100% energy) of the beams measure 160 – 340- μrad compared to a design goal of 120 μrad . The increased beam divergence observed is consistent with the observed spatial energy distributions of the multiple modes exiting the 62.5 μm fiber. The inferred beam footprints range nominally from 7.5 – 16 m. Using these values the best, nominal and worst-case link budget predictions shown in Table 2 were made.

Table 2 Showing the link analysis for transmission of a single beacon laser from TMF to SP

LINK MARGIN	Best Case (dB)	Nominal Case (dB)	Worst Case (dB)
Transmitted Power	11.46	11.46	11.13
System Loss	-36.7	-41.7	-49.2
Atmospheric Loss	-39.7	-45.7	-54.2
Pointing Loss	-39.7	-45.7	-57.2

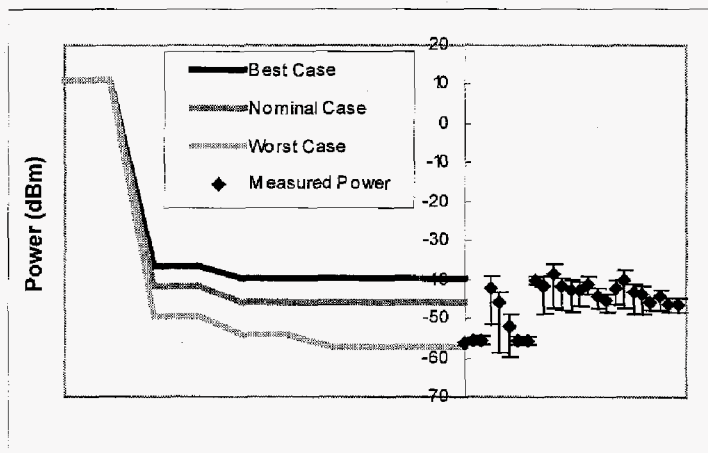


Figure 4 A graphical representation of the link uncertainties for a single 780 nm laser beam transmitted from TMF to SP compared to actual measured power at SP

The transmitted power in Table 2 is based on measured values. The system loss represents relay optics and space transmission losses (reasonable estimates for the TMF telescope mirrors were used). Full width beam divergences of 160, 250 and 340 μ rad were used for the best, nominal and worst case.

The atmospheric transmission was assumed to be 3, 4 and 5 dB attenuation for the best, nominal and worst case. A 3 dB pointing loss was assumed for the worst-case while zero pointing losses were allocated to the best and nominal case. Figure 4 shows a comparison of the prediction with measured average powers. The error bars represent the standard deviation recorded for these measurements. Excellent agreement is apparent between predicted and measured powers. Furthermore, the distribution of measured powers suggests that 75% of the time the 5-6 dB uncertainties predicted between the best and nominal case is valid.

As a final test received He:Ne power was measured. Note that He:Ne beam divergence is $\sim 800 \mu$ rad otherwise the relay optics losses and atmospheric transmission are assumed the same. The predicted nominal average received power is -58.8 dBm versus measurements ranging between -58.9 to -58.3 dBm.

3.12 Multi-Beam Scintillation

Reduction of the scintillation index (SI) due to non-coherent averaging of multiple beams was validated by recording the received power (20-second durations) through the spotting telescopes at SP for 1, 2, 4, 6 and 8 beams transmitted sequentially from TMF. These measurements were made for two nights in June 2000. Figure 4 shows a summary of the normalized variance or SI obtained from an analysis of the recorded data. The measured SI's for each individual beam showed some variation as indicated by the error bars in Figure 4. These error bars represent the standard deviation of the measured SI values. Bearing in mind that the irradiance distributions for single beams, where $SI \geq 0.5$, can only be approximated by a lognormal function⁷ the multi-beam averaging measurements are compared to a simulated lognormal averaging. This is shown by the solid curve in Figure 4, obtained by averaging lognormal distributions generated using Mathcad software with means and standard deviations similar to the measured irradiance distributions. The solid line predicts an eight-fold reduction in the SI as was concluded by previous analysis⁸. In the measurements of Figure 4 approximately fourfold reduction was achieved. The deviation from the approximate theory is attributed to imperfect spatial overlap of the beams resulting in certain beams weighting the average that is realized. In other experimental studies involving horizontal path measurements over a 5 Km range a threefold⁹ intensity variance reduction was reported when averaging nine argon laser beams. During the GOLD (ground-to-geo-stationary (GEO) satellite) experiment⁸, a four-fold reduction in SI was inferred when using four beams. The eight-beam SI reported in Figure 4 and representing measurements made in June 2000 were reproduced in subsequent night campaigns conducted during August and September 2000.

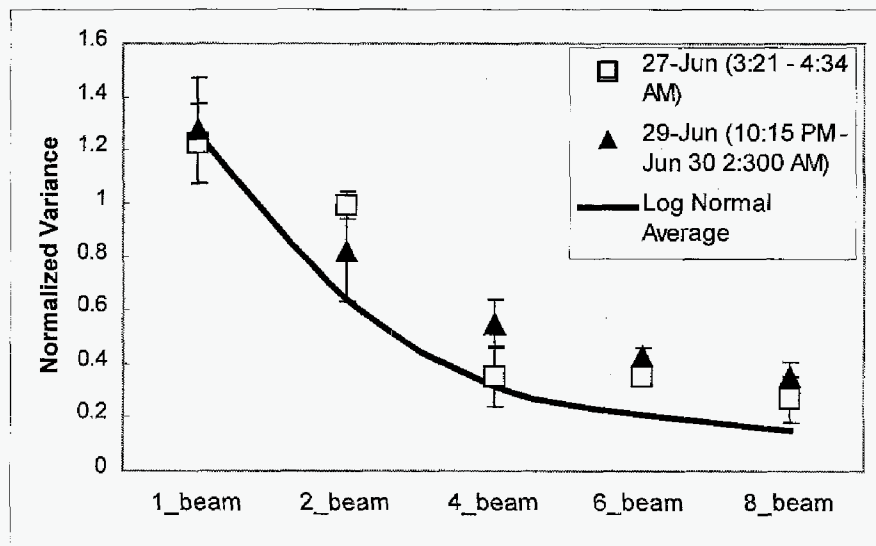


Figure 4 Showing the measured reduction of normalized variance or scintillation index (SI) as a result of multi-beam averaging, the solid line is a simulated average of lognormal distributions

3.13 Fade Characteristics

The eight-beam scintillation measured during August and September 2000 was used to determine the beacon fade characteristics. The fade probability corresponding to each data set acquired (20-second record of irradiance at 2500 samples per second) by the spotting telescopes was determined from the fraction of time the signal level fell below a threshold set by the background level. Figure 5a shows a plot of the fade probability versus SI for data gathered during August and September, 2000. Theoretical fade probability^{2,7} plots of log-normally distributed irradiance for 4, 6 and 8-dB fade depths are shown in Figure 5a. For data sets that displayed no fades over the 20-second duration the probability was made equal to 2E-5, though it could have been lower. Larger than 80% measurements are consistent with the theory and suggest a distribution of fade depths. The fade depths were estimated from the measured data by finding the difference between the average beacon signal and the background threshold in dB. A histogram showing the distribution of observed fade depths is shown in Figure 5b along with the cumulative distribution function. The histogram verifies that the most frequently observed fade depths were 7 dB. The normalized irradiance power spectrum^{2,7} was used to determine the quasi-frequency and this quantity in turn allowed a determination of the mean number of fades and the mean fade duration.

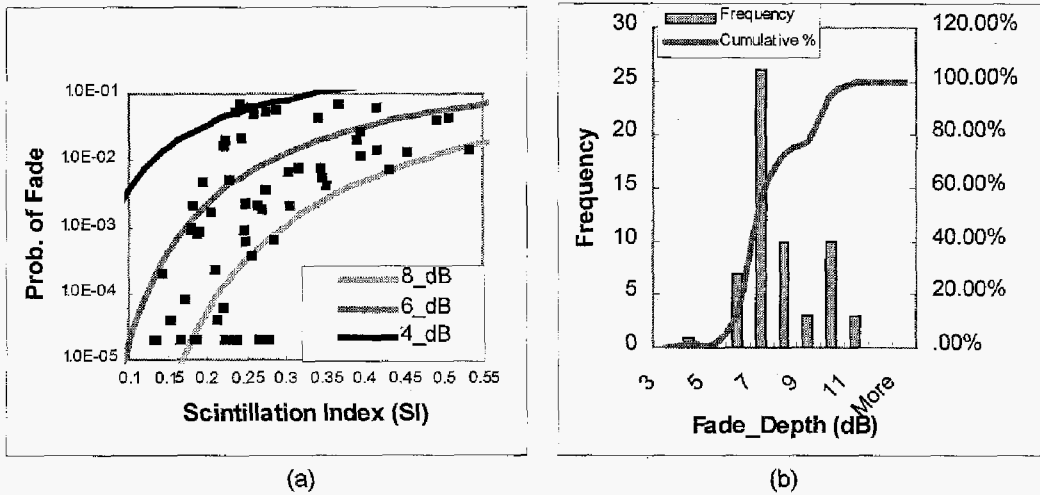


Figure 5 (a) Fade probability versus SI (small squares) compared to theoretical predictions for 4, 6 and 8-dB fade depths (b) Histogram of observed fade depths along with cumulative distribution function (CDF).

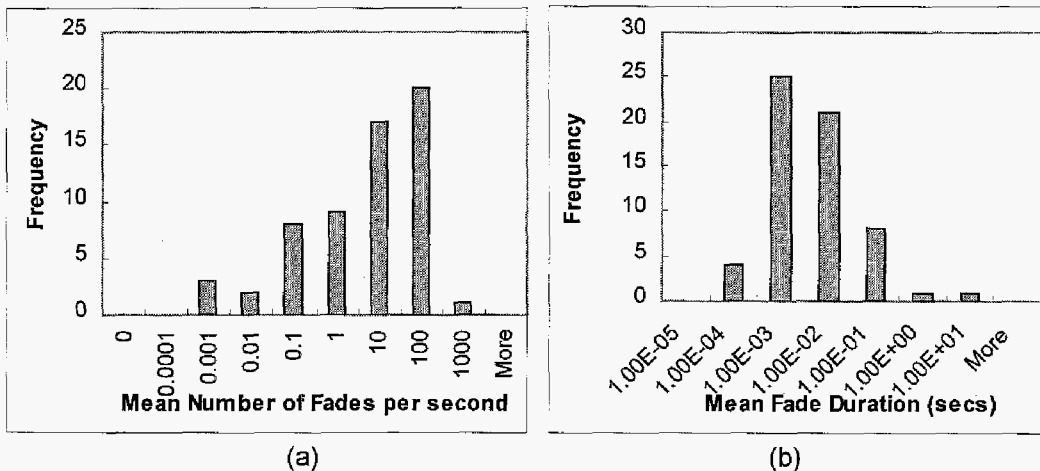


Figure 6 (a) Distribution of measured mean number of fades and (b) mean fade duration

As Figure 6 shows between 1 and 100 mean fades per second and 1 and 10 milliseconds mean fade durations were observed in our measurements.

3.2 Optical Communications Demonstrator (OCD)

Following the alignment procedure described in Section 2.1 the OCD at SP acquired the eight-beam beacon with characteristics described in the preceding section. Both open loop acquisition and closed loop fine tracking in order to compensate for the atmosphere induced phase tilt of the beacon were tested.

3.21 Open loop acquisition

During open loop acquisition of the beacon with OCD, the charge-coupled device (CCD) tracking sensor records the spot intensity and centroid while updating at 1-kHz. Beacon images can also be recorded at lower frame rates. The incident irradiance on OCD is independently monitored by the spotting telescopes. These power measurements indicate an average irradiance of $\sim 0.1 \text{ nW/cm}^2$ at the OCD aperture. The irradiance was adjusted by attenuating the beacon broadcast from TMF, and was set in order to prevent fades or excessive surges in power on the OCD tracking sensor. The recorded beacon images revealed 4×4 to 8×8 pixels (~ 40 to $80 \mu\text{rad}$) spots with a Gaussian point spread functions. This compares to near diffraction limited 3×3 pixel spots measured in the laboratory. Examining a series of recorded beacon spots shows that $\sim 30\%$ of the spots were saturated. The most severe cases of saturation involved 4 – 5 central pixels. This is consistent with previous laboratory characterization where the required irradiance at the aperture was found¹⁰ to be $\sim 20 \text{ pW/cm}^2$ in order to prevent saturation of a 3×3 pixel spot. In spite of saturating the CCD pixels at times, this irradiance level was found to be effective in eliminating fades altogether. Moreover, even the saturated beacon spots yielded centroid values without noticeable "blooming". Ideally, a larger dynamic range for the OCD sensor is desirable in order to handle the irradiance fluctuations encountered, however, by allowing the tracking sensor to saturate by an "acceptable" amount, fades can be eliminated and reasonable tracking performance can be obtained, as described in what follows.

Analysis of open loop tracking showed that the beacon intensity fluctuations as measured by the OCD tracking sensor was typically $\sim 11 - 12 \text{ dB}$ with negligible fades for the 10 second duration measurements. The rms beacon spot motion was $\sim \pm 8 \mu\text{rad}$.

3.22 Closed loop tracking

With fine tracking turned on the OCD tracking sensor records 5-second snap-shots of beacon and transmitted laser spot intensities and centroids, updated at 1 kHz.

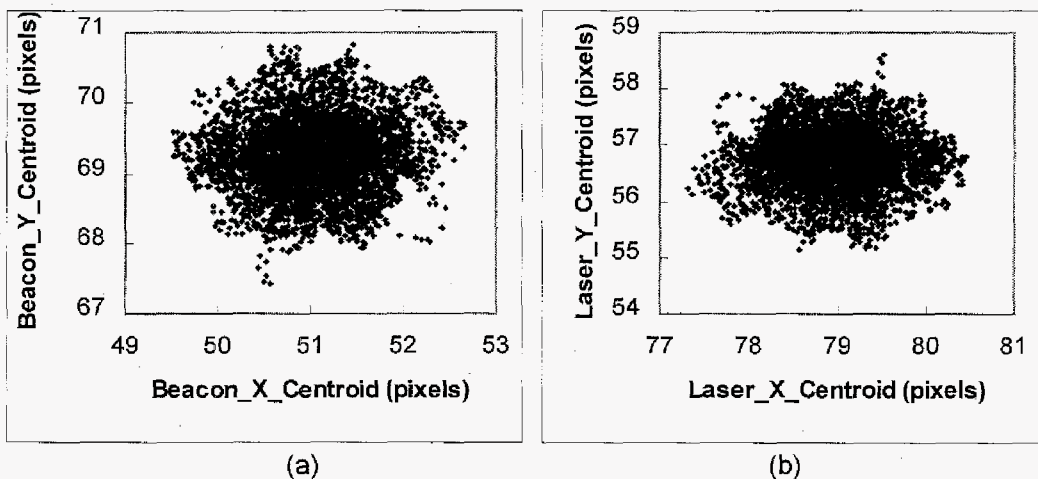


Figure 7 (a) The beacon centroid motion on the tracking sensor (b) corresponding OCD communications bore-sight laser spot centroid. Both centroid motions represent a 5-second snap shot of data recorded at 1-kHz update rate.

The primary function of the OCD fine-tracking control loop is to track the beacon position using the updated beacon centroids logged by the CCD and feeding this information to the fine steering mirror so that it can update the communications laser fine pointing to preserve a fixed offset between beacon and bore-sight centroids. Figure 7a shows a 5-second duration of recorded beacon centroids and the corresponding bore-sight laser centroid positions are shown in Figure 7b. The reduced size used to represent Figure 7 make discerning the qualitative similarities in the two spot patterns difficult. The nature of the OCD tracking loop is such that in response to any beacon motion, the bore-sight laser spot moves in the opposite direction so that adding the

incremental changes in x and y directions should cancel out exactly. However, imperfect loop performance results in some uncompensated residual motion. Figure 8 shows histograms of the residual x and y motion resulting from summing the incremental x and y motion for each frame of data recorded.

The histograms in Figure 8 are fitted to Gaussian distributions and the rms residual motion determined from the fits is ± 0.11 and ± 0.18 pixels in the X and Y directions. The larger value in the Y-direction is attributed to an anomaly in the CCD readout. Based on the plate scale of the OCD this corresponds to ± 1.1 and $\pm 1.8 \mu\text{rad}$ of uncompensated error. This tracking performance is typical of a number of observations made in August and September of 2000.

The motions of the spots on the CCD are best described by a determination of the power spectral densities (PSD). Figure 9 shows PSDs for the X and Y centroid motion. For comparison, Figure 9 also includes Olympus spacecraft vibration PSD¹¹ that indicates the beacon motion induced by atmospheric turbulence across the horizontal range used is comparable to spacecraft jitter typically used to validate fine tracking performance of optical communications terminals.

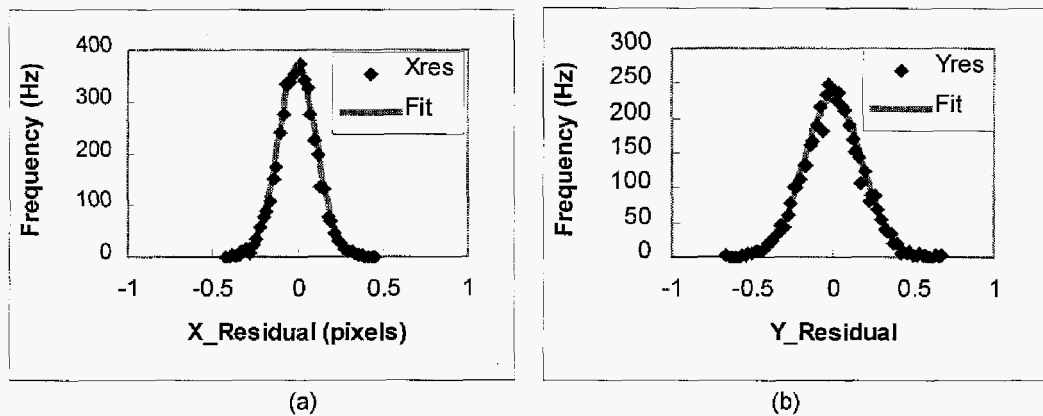


Figure 8 (a) The residual motion in pixels after adding the incremental X centroids of the beacon and bore-sight spot recorded on the CCD (b) same for the Y centroids

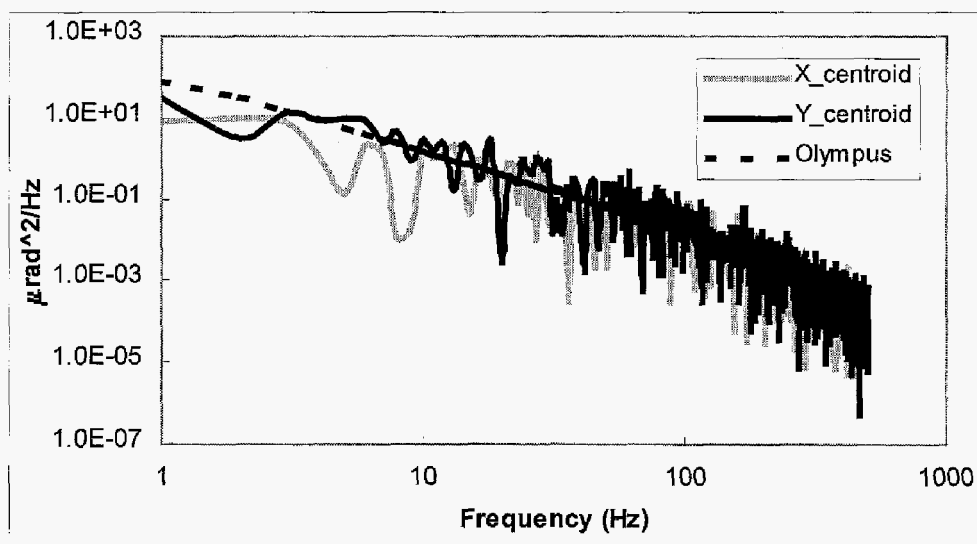


Figure 9 Displays the PSDs for the x and y centroid motion measured along with the PSD for the Olympus Spacecraft vibration PSD.

The OCD fine steering control loop was independently characterized in the laboratory using the upgraded fine steering mirror and the derived model is shown in Figure 10 where the 0-dB bandwidth is ~ 70 Hz. The uncompensated motion can be determined using the relationship:

$$\theta_{\text{rms}} = \sqrt{\int S(f) |R(f)|^2 df}$$

where $S(f)$ is the angular motion beacon power spectral density (Figure 8) and $R(f)$ is the tracking –control-loop rejection in the frequency domain (Figure 10). Upon applying this relation to the data shown above θ_{rms} was found to be $3.4 \mu\text{rad}$ compared to the ± 1.1 and $\pm 1.8 \mu\text{rad}$ directly determined from Figure 8 above.

3.3 TMF Receiver

The active tracking of the beacon by the OCD results in an 844 nm communications beam with on-off key modulation at 400 Mbps being pointed back to TMF. The power received at TMF validates the uncertainties in the optical link from SP to TMF. In addition, the received signal is used to monitor the pupil and focal plane images, as well as, test eye patterns and bit-error rates.

3.31 Power received at TMF

Table 3 shows the link analysis for the OCD laser transmitted from SP to TMF. The transmitted power shown in Table 3 was measured at the optical fiber end delivering the laser to OCD. The net system loss results after optical transmission and space loss added to antenna gains at the transmitter (OCD) and receiver (0.6 m TMF telescope). All of these quantities are known within ~ 1 dB of uncertainty. Atmospheric transmission

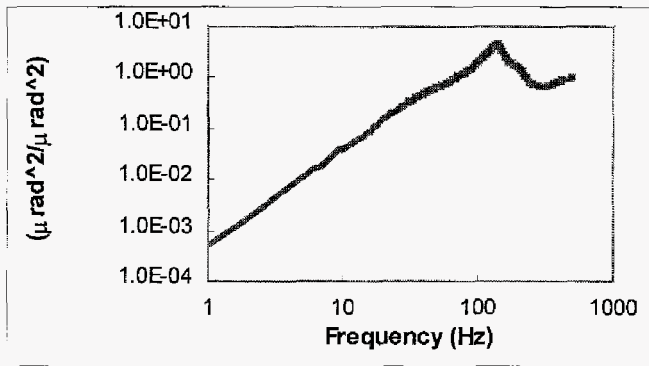


Figure 10 The derived model for the OCD control loop showing a 0-dB bandwidth of ~ 70 Hz for both the x- and y-axis motion.

at zenith for 780 and 852 nm differs¹² by $\sim 1\%$, so for the purposes of our link analysis they have been assumed the same. The OCD beam divergence observed in the laboratory using LTES prior to the ground-to-ground campaign was $22 \times 17 \mu\text{rad}$, in agreement with previous measurements¹⁰. The beam footprint received from SP was projected on the TMF telescope-building wall and the visual extent of this spot when observed through an infra-red (IR) viewer was 2.1×1.88 m. The asymmetry in the spot size observed in the laboratory was

Table 3 Showing link analysis for OCD laser transmission from SP to TMF

	Best Case (dB)	Nominal Case (dB)	Worst Case (dB)
Transmitted Power	8.45	8.45	8.45
System Loss	-4.51	-4.87	-5.56
Atmospheric Loss	-7.52	-8.85	-10.79
Beam Spread Loss	-9.74	-11.97	-14.91
Pointing Loss	-9.74	-14.98	-44.91

preserved, however, the expected footprint size due beam divergence over 46.8 Km is expected to be 1×0.8 m. The additional beam spreading is attributed to refractive effects caused by the atmosphere and is budgeted as a beam spreading loss in Table 2. The best case pointing loss is neglected assuming perfect on-axis pointing, whereas for the nominal and worst case 3 and 28 dB is used. The worst case pointing loss is based upon the third lobe of the OCD far-field Airy pattern being incident upon the telescope. Theoretically, the third Airy lobe or ring is down in intensity by 28 dB and spatially 3 times the radius of the first ring away from the beam center¹³.

Figure 11 shows the measured power values plotted next to a graphic representation of the link analysis presented in Table 2. The agreement is very good. The single power measurement of -40.3 dB validates the -28 dB worst case pointing loss. This data point was obtained is by starting with OCD aligned optimally and then

stepping the fine steering mirrors (34 μrad in X and 5 μrad in Y) which corresponds to \sim three times the first bright ring radius of 11 μrad . Moreover, visual examination of the spot provided an estimated 3.6 m displacement of the spot from the telescope axis that is close to three times the observed spot radius. These measurements demonstrate that a very large pointing margin exists.

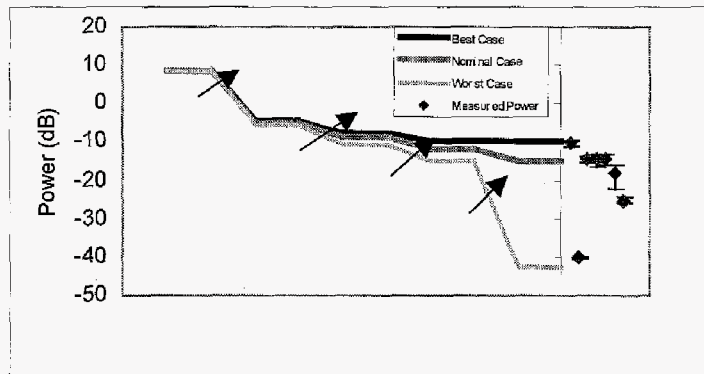


Figure 11 A representation of the predicted link uncertainties compared to the measured power received at TMF

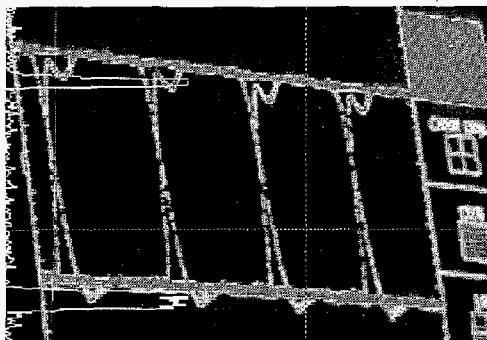
3.32 Atmospheric effects on communications signal

The scintillation index was determined from the irradiance fluctuations recorded at the Coude focus of the TMF telescope. The SI observed varied between 0.16 and 0.27. This compares to a theoretical prediction² of 0.08 – 0.11 taking into account the expected aperture averaging from the 0.6-m diameter telescope receiver. The focal spot sizes of the received signal from SP to TMF were also recorded. The average spot sizes measured at the focal plane are 325-375 μm in diameter consistent with a Fried parameter, $r_0 \sim 1\text{-}2\text{ cm}$. r_0 values of 3-4cm are inferred from the measured spot sizes on the OCD focal sensor.

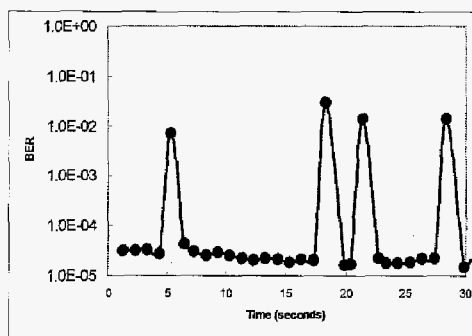
Another interesting comparison is the rms phase tilt. At TMF the extent of the angular phase tilt judged by the rms centroid motion on the focal plane is 56-66 μm . This translates to an rms angular phase tilt of 18-21 μrad . Theoretically, the prediction is 27 μrad assuming a C_n^2 value of $1\text{E-}17\text{ m}^{-2/3}$. On the other hand the rms motion observed at OCD is 12-13 μm which corresponds to an rms angular phase tilt of 6.4 μrad . This compares to a theoretical rms value value of 1 μrad .

3.33 Overall link performance

Satisfactory eye patterns were recorded at TMF and a representative is shown in Figure 12a. These were recorded on a high bandwidth oscilloscope after performing clock and data recovery on the APD output signal. The same signal was connected to the receiver module of a bit error rate tester (BERT) and a typical output of the BERT is shown in Figure 12b where the best bit error rates are $\sim 1\text{E-}5$. The BERT actually provides the BER averaged over 1 second.



(a)



(b)

Figure 12 (a) representative eye-pattern recorded on high bandwidth oscilloscope

4. CONCLUSIONS

Results of the horizontal link campaign performed during the nights of June 27-30, August 2-3 and September 13 -15 have been presented above. The extent of scintillation index reduction achievable using a multi-beam beacon comprised of eight multi-mode fiber coupled sources was close to a factor of 4. The uncompensated tracking errors which are predicted to be $\sim 3 \mu\text{rad}$ were found to be 2-3 μrad . The slight difference in predicted and observed performance is attributed to model assumptions.

ACKNOWLEDGEMENT

The help provided by Dr. Jim Young (JPL, TMF), Dr. Shinak Lee, Mr. Jason Beebe, Mr. Albert Vega, Mr. Beckett Madden-Woods and Mr. William Liu is gratefully acknowledged. Thanks are due to Ms. Julie Kessler of the USDA, Forest Service, Ranger Station. The research described was carried out with funding from the TMOD Technology Program Office, Jet propulsion Laboratory, California Institute of Technology, under contract with the National Aeronautics and Space Administration.

REFERENCES

1. A. Biswas, J. Cenicerros, M. Novak, M. Jeganathan, A. Portillo, D. Erickson, J. Depew, B. Sanii, J. Lesh, "45 Km horizontal path optical link experiment," Proceedings of SPIE, Free-Space Laser Communications Technologies XI [Ed. G. Stephen Mecherle], 3615, 43, 1999.
2. A. Biswas and S. Lee, "Ground-to-Ground Optical Communications Demonstration," The Telecommunications and Mission Operations Progress Report, [Ed. J. Yuen] 42-141, May 15, 2000, Jet Propulsion Laboratory, California Institute of Technology, Pasadena, California
3. J. Lesh, C. -C. Chen and H. Ansari, "Lasercom system architecture with reduced complexity," U. S. Patent Number 5,517,016, May 1996.
4. M. Jeganathan, A. Portillo, C. Racho, S. Lee, D. Erickson, J. Depew, S. Monacos and A. Biswas, "Lessons Learnt from the Optical Communications Demonstrator (OCD)," Proceedings of SPIE, Free-Space Laser Communications Technologies XI [Ed. G. Stephen Mecherle], 3615, 23, 1999.
5. Robert R. Beland, "Propagation through Atmospheric Optical Turbulence," Volume 2 Atmospheric Propagation of Radiation [Ed. Frederick G. Smith], The Infrared & Electro-Optical System Handbook, SPIE Optical engineering Press, Bellingham, WA, USA, 201, 1993
6. Peter Duffett-Smith, "Practical Astronomy with your calculator," 36-65, Cambridge University Press, 1981.
7. Larry C. Andrews and Ronald L. Phillips, "Laser beam Propagation through Random Media," SPIE Optical Engineering Press, Bellingham WA, 1998.
8. M. Jeganathan, M. Toyoshima, K. Wilson, J. James, G. Xu and J. Lesh, "Data Analysis results from the GOLD Experiments," Free-Space Laser Communications technologies IX, Proceedings of SPIE, [Ed. G. Stephen Mecherle] 2990, 70-81, 1997.
9. C. Higgs, H. Barclay, D. Murphy, and C. A. Primmerman, "Multibeam Illumination," Lincoln Laboratory Journal, 11, 8-22, 1998.
10. M. Jeganathan, S. Monacos, "Performance analysis and electronics packaging of the Optical Communications Demonstrator," Proceedings of SPIE, Free-Space Laser Communications Technologies XI [Ed. G. Stephen Mecherle], 3226, 33, 1998.
11. M. Wittig, L. van Holtz, D. E. I. Turnbridge and H. C. Vermuelen, "In-Orbit Measurements of Microaccelerations of ESA's Communication Satellite OLYMPUS," Proceedings of SPIE, Free-Space Laser Communications Technologies XI [Ed. G. Stephen Mecherle], 1218, 205, 1990.
12. A. Berk, L.S. Bernstein, G.P. Anderson, P.K. Acharya, D.C. Robertson, J.H. Adler - S. M. Golden, "MODTRTAN cloud and multiple scattering upgrades with applications to AVIRIS," Remote Sensing of Environment, 65, 367-375, 1998.
13. M. Born and E. Wolf, "Principles of Optics, 439-443, 7th Edition, Cambridge University Press, 1993.